

Non-Gaussian Spikes from Chaotic Billiards in Inflation Preheating

J. Richard Bond¹, Andrei V. Frolov², Zhiqi Huang¹, and Lev Kofman¹

¹ CITA, University of Toronto, 60 St. George Street, Toronto, ON M5S 1A7, Canada and

² Physics Department, Simon Fraser University, Vancouver, BC V5A 1S6, Canada

(Dated: March 2, 2022)

A new class of non-Gaussian curvature fluctuations $\zeta_{pr}(\mathbf{x}) \equiv \delta N(\chi_i)$ arises from the post-inflation preheating behaviour of a non-inflaton field χ_i . Its billiard-like chaotic dynamics imprints regular log-spaced narrow spikes in the number of preheating e-folds $N(\chi_i)$. We perform highly accurate lattice simulations of SUSY-inspired quartic inflaton and coupling potentials in a separate-universe approximation to compute $N(\chi_i)$ as a function of the (nearly homogeneous) initial condition χ_i . The super-horizon modes of $\chi_i(\mathbf{x})$ result in positive spiky excursions in ζ_{pr} and hence negative gravitational potential fluctuations added to the usual sign-independent inflaton-induced perturbations, observably manifested in large cosmic structures and as (polarized) temperature CMB cold spots.

PACS numbers: PACS: 98.80.Cq, CITA-2009-3, astro-ph/0903.3407

During early universe inflation, vacuum fluctuations in all light fields χ are transformed on super-horizon scales into homogeneous and isotropic Gaussian random fields. These are fully defined by their power spectra $\frac{d\sigma_\chi^2(k)}{d\ln k} \equiv \langle |\chi_k|^2 \rangle \frac{k^3}{2\pi^2}$, whose magnitude, $\sim [H/(2\pi)]^2$, is related to the Hubble parameter H at expansion factor a when Ha first equals the wavenumber k in question. In standard scenarios, metric curvature fluctuations ζ_ϕ are derived from an inflaton ϕ and are nearly Gaussian and often nearly scale invariant, with power $d\sigma_\zeta^2(k) \approx d\sigma_\phi^2(k)/(2M_P^2\epsilon)$, in terms of the acceleration parameter $\epsilon \equiv -\frac{d\ln H}{d\ln a}$ and the reduced Planck mass $M_P \equiv 1/\sqrt{8\pi G_N}$ [1]. Observational constraints on ϵ are < 0.03 at the 95% confidence limit from the large angle cosmic microwave background radiation (CMB), hence ζ is considerably amplified over ϕ . Alternative mechanisms utilizing light “non-inflatons” χ must overcome this ϵ effect. Examples are “curvatons” which temporarily dominate the energy density after inflation [2], and fields which induce spatial variations of couplings which modulate the timing of the now-inhomogeneous post-inflation (p)reheating [3], but are not gravitationally dominant.

The ζ -source first proposed in [4] and studied here is nonlinear resonant preheating inducing expansion factor variations from the end of inflation at $\epsilon = 1$ to when the equation of state settles to $w = 1/3$. A sample framework [5] for this has a potential $V = \frac{1}{4}\lambda\phi^4 + \frac{1}{2}g^2\phi^2\chi^2$, with inflation driven by the first and particle creation by the second term. If g^2/λ is tuned to be $\sim \mathcal{O}(1)$, the non-inflaton $\chi(\mathbf{x})$ is light during inflation and accumulates quantum fluctuations substantially varying on scales much greater than the Hubble scale at the end of inflation $H_e \sim 10^{-7}M_P$. We note that $g^2/\lambda=2$ corresponds to a SUSY model. On scales shorter than H_e^{-1} , this $\chi(\mathbf{x})$ is nearly homogeneous defining “separate universes” with specified χ_i as initial conditions for lattice simulations of the fully coupled fields to determine the nonlinear evolution w , which imprints itself on $\ln a(\chi_i)$. The resulting curvature perturbations

$\zeta_{ph}(\mathbf{x})$ are differences in the number of e-folds on uniform Hubble (*i.e.* uniform energy density) time hypersurfaces, $\zeta \equiv \delta \ln a|_H = \delta N(\chi_i)$ [6]. If such variations exist, they would be in addition to the standard ones. Preheating in the model begins with parametric resonance amplifying the fluctuations $\chi_k(t)e^{ik\cdot\vec{x}}$ describing vacuum excitations of χ -particles. The problem can be reduced to a flat space-time model by a conformal transformations, $\chi_k(t)$ obeys an oscillator equation with a periodic frequency controlled by the background inflaton oscillations $\phi(t)$ with (conformal time) period $T \approx 7.416$ [5]. In the resonant bands, $\chi_k(t) \sim e^{\mu_k t}$ is unstable, an exponent μ_k is a function of g^2/λ and k . If $g^2/\lambda \sim 2$, the maximum of μ_k in the first resonant band is located close to $k = 0$. Hence a nearly homogeneous χ_i will be exponentially unstable in each separate universe, and soon becomes entangled in the complicated mode-mode dynamics of preheating driven by the back-reaction effects of copiously produced χ and $\delta\phi$ particles. To determine $\delta N(\chi)$ at the part per million level, we need non-linear lattice simulations with energy conservation accuracy (ECA) well below this. The early attempt by [4] used first-order lattice simulations with ECA $\sim 10^{-4}$ to claim an effect at the level $\delta N \sim 10^{-3}$, with a dominantly-quadratic form $\delta N \approx f_\chi \chi_i^2$ characterized by a constant f_χ similar to f_{NL} used in non-gaussianity (nG) studies of the CMB sky [7]. We do not confirm the large quadratic nG of [4], but do find a nontrivial $\delta N(\chi_i)$ with a regular sharp-spiked pattern at the observationally interesting $\sim 10^{-5}$ level, as shown in Fig. 1, with a radically different impact on the sky than the f_{NL} story. Although our discovery of the spiked $\delta N(\chi_i)$ function was a truly numerical one, a posteriori we can explain it by a combination of chaotic zero-mode dynamics after t_e and the abrupt onset of inhomogeneous nonlinearity at a preheating time t_{pr} , allowing us to conjecture for which models it works.

To accurately compute the very low levels of $\delta N(\chi_i)$, especially since we are in finding and validation mode for such tiny effects, we needed to go well beyond the ECA

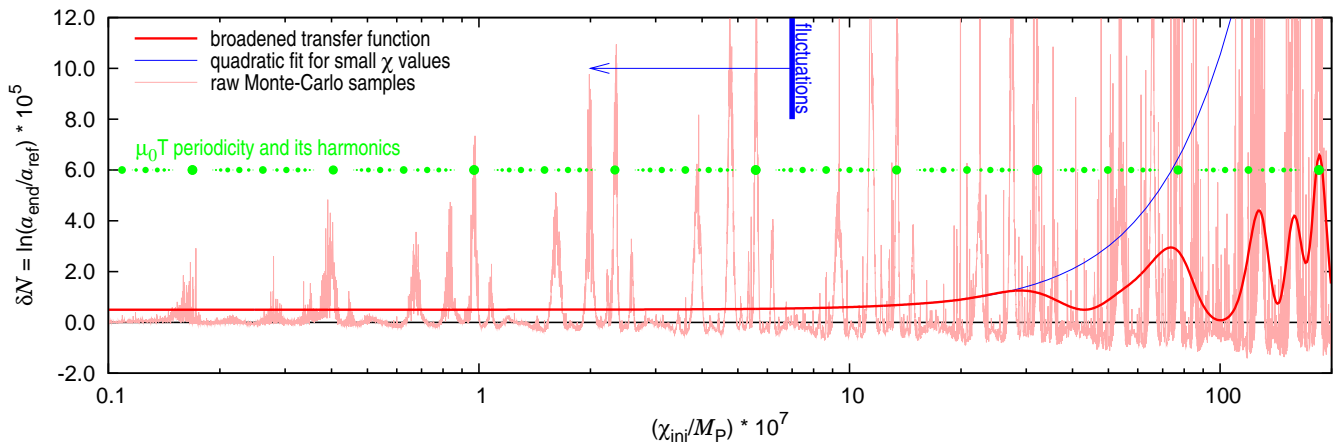


FIG. 1: The structure of $\delta N(\chi_i)$ on uniform Hubble hypersurfaces probed with $\sim 10^4$ lattice simulations from the end-of-inflation through the end-of-preheating for varying homogeneous χ_i initial conditions, for $g^2/\lambda = 2$. The periods $n\mu_0 T$ in $\ln \chi_i$ are marked by the large green circles, and the higher harmonics (revealed by the Fourier analysis) by smaller green circles. These locate the spikes in $\delta N(\chi_i)$. The effective field $(F_{\text{NL}}|\chi_b + \chi_{>h})$ marginalized over high spatial frequencies with $\sigma_{\text{HF}} = 7 \times 10^{-7} M_P$ (vertical line) yields the solid curve. A quadratic fit, $f_\chi(\chi_b + \chi_{>h})^2$, is also shown. An issue for our Hubble patch is whether the ultra-large scale $\chi_{>h}$ is large enough that the large scale structure fluctuations about it, $\pm\sigma_{b<h}$, encompass smoothed peaks in field space, or not. A typical value for $\sigma_{b<h}$ is $\sim 3 \times 10^{-7} M_P$.

practically achievable in second-order preheating codes (typically $\sim 10^{-3}$ for LATTICEASY [8] and $\sim 10^{-5}$ for DEFROST [9]). We developed a new high-order symplectic PDE solver with adaptive time steps, which can reach machine precision levels (ECA $\sim 10^{-13}$) to address this problem. In retrospect, we find that ECA of 10^{-7} would suffice, which is achievable with shorter timesteps in DEFROST. The lattice simulations begin at expansion factor a_e when $\epsilon = 1$; we have shown that variations of the start do not effect results. The calculations are stopped at a uniform Hubble value H_f when the $w = p/\rho$ is nearly $1/3$, the radiation-dominated value. Although the average w is $\approx 1/3$, it has small oscillations during preheating, leading to a fluctuations to average over to determine $N(\chi_i)$ for use in the curvature formula. To deal with this, we used an accurate extrapolation template for the averaged $a(t)$ or, for superb accuracy, a Kaiser window filter to suppress high frequency oscillations in $a(t)$ by a factor 10^{-8} . With either, we showed that provided we calculate for 5-6 e-folds after a_e , the specific H_f is not important. An accuracy test was to show δN is effectively zero ($\ll 10^{-6}$) and not modulated by χ_i for g^2/λ out of the resonant band, *e.g.*, at $g^2/\lambda = 1$ and 3 , for which $\mu_0 = 0$. With the symplectic code, we ran a 256^3 lattice with a box size $64/H_e$ to check that our conclusions derived using a very large number of lower resolution simulations using DEFROST to build up statistics in χ_i are accurate. The essential effects can indeed be captured with lower resolution and box size. Fig. 1 showing a spiky pattern in $\delta N(\chi_i)$ for $g^2/\lambda = 2$ was produced with $11563 \cdot 32^3$ -simulations with box size $20/H_e$. The amplitude of spikes increases as χ_i increases. The spikiest pattern is at $g^2/\lambda = 1.875$, with the spikes broadening away from that, finally disappearing at the $g^2/\lambda = 1$ and 3 borders.

For Fig. 1, we explored a large range in input χ_i/M_P , from 10^{-8} up to 2×10^{-5} . $\chi_i(\mathbf{x}) = \chi_{<h} + \chi_{>h}$ has a sub-horizon contribution $\chi_{<h}$ from eigenmodes with wavenumbers between $k_e \sim H_e a_e$ to the current horizon scale, $k_h \sim H_h a_h$, and a super-horizon contribution $\chi_{>h}$ with waves from k_h to a k_{min} whose value will depend upon the inflation model. The corresponding variances are $\sigma_{<h}^2 = \int_{k_h}^{k_e} d\sigma_\chi^2$ and $\sigma_{>h}^2 = \int_{k_{\text{min}}}^{k_h} d\sigma_\chi^2$. Over > 100 e-folds, $d\sigma_\chi^2$ is nearly constant for $1 < g^2/\lambda < 2$, drops substantially as $a \rightarrow a_e$ for $g^2/\lambda = 0$ ($\sim \phi^4$ as expected), and actually rises for $g^2/\lambda = 3$. The least number of e-folds $\ln a_h/a_e$ must exceed $\sim 50 - 60$, and since $H > H_e$ during inflation, $\sigma_{<h}^2 \gtrsim \ln k_e/k_h [H_e/(2\pi)]^2$ gives a $\chi_{<h}$ enhanced over H_e by $\sim \sqrt{55}$. The super-horizon power, $\sigma_{>h}^2 \gtrsim \ln k_h/k_{\text{min}} [H_e/(2\pi)]^2$ is also log-enhanced, and considerably so in our illustrative $\lambda\phi^4$ example. Thus, the log factors give larger χ_i , including a $\chi_{>h}$ random number which is nearly constant within our Hubble patch, but has a $\sim \pm\sigma_{>h}$ patch-to-patch ‘‘cosmic variance’’.

We now show how the features of $\delta N(\chi_i)$ can be understood qualitatively from trajectories in the two-dimensional space of homogeneous modes $(\phi(t), \chi(t))$. The excited inhomogeneous degrees of freedom do back-react on these $k \approx 0$ modes, but only later in the evolution, *e.g.*, at $t \sim 10T$ for $g^2/\lambda = 2$. The $(\phi(t), \chi(t))$ space is effectively bounded by potential energy barriers $\frac{1}{4}\lambda\phi^4 + \frac{1}{2}g^2\phi^2\chi^2 = \text{const}$, as shown in Fig. 2. Initially the trajectories oscillate mostly in the ϕ direction, with only very small initial amplitudes in χ , as illustrated in the insets in Fig. 2. These oscillations are akin to billiard motions between the potential walls. Precession of the initial oscillations causes the χ amplitude to grow exponentially in a chaotic manner: $\chi(t) = \chi_i e^{\Lambda t}$, where Λ is

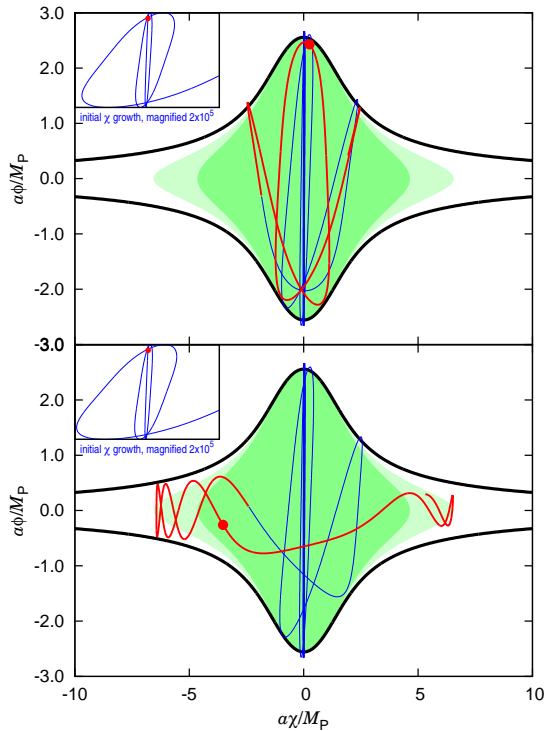


FIG. 2: Billiard trajectories of the $k = 0$ modes $\phi(t)$ and $\chi(t)$ within the $\lambda\phi^4/4 + g^2\chi^2\phi^2/2$ potential well. Upper panel has a “no-spike” initial value $\chi_i = 3.6 \times 10^{-7} M_P$, and the bottom panel has a “spiky” $\chi_i = 3.9 \times 10^{-7} M_P$. The solid curves are the (fuzzy) potential wall without the inclusion of mass terms induced by field nonlinearities; the pale green and brighter green border areas include the induced masses at the instances $t = 10.8T$ and asymptotically. Thin and thick parts of the trajectories denote before after $t = 9.7T$, and up to $11.8T$, with the circle on it at $t = 10.8T$. The inserts in the left upper corners of the panels show the first several periods of linear oscillations.

the Lyapunov exponent. This gives us new insight on the parametric resonant $k = 0$ solution in terms of the Lyapunov instability. For $g^2/\lambda = 2$, we find $\Lambda = \mu_0 = 0.235$. This conjecture also works for the cases in which $k = 0$ is not in the resonant band; *e.g.*, for $g^2/\lambda = 3$ we have $\mu_0 = 0$ and do indeed find periodic trajectories so $\Lambda = 0$.

As χ grows beyond the linear regime, the bouncing billiard experiences the negative curvature of the potential walls and a bifurcation of the trajectories occurs, with a few entering the arms in between walls, and most do not. If there were only homogeneous modes the impact of this would be temporary because eventually all trajectories would be chaotically mixed. However, the excitation of the inhomogeneous modes result in exponential growth of $\langle \chi^2 \rangle$ and $\langle \delta\phi^2 \rangle$, as $e^{2\mu_* t}$ and $e^{4\mu_* t}$ respectively, where μ_* is an effective resonant exponent [5]. These induce enhanced effective masses in the fields, abruptly changing the potential, with the arms in between walls closing exponentially quickly, as shown in Fig. 2. The trajectories which happen to get into the arms before arm-closure evolve very different from those which never get

into the arms. The billiard picture breaks down when the gradient terms in χ and $\delta\phi$ occur, at arm-closure time, but the bifurcation determined by the initial conditions at the linear stage has already happened. The two pre-closure classes of in-arm and not-in-arm trajectories result in different equations of state, and hence a χ_i -dependent $\delta N(\chi_i)$. In-arm trajectories experience kinetic energy kicks from the closing arms, which translates into a transient decrease in w , inducing a jump in δN . The no-spike trajectories of the upper panel of Fig. 2 are much more numerous than the rarer sort in the lower panel corresponds that give spikes. The billiard picture predicts the spike pattern as one periodic in $\ln \chi$ which works extremely well: the same “spiky” trajectory labeled by χ_i is repeated for initial values $\chi_i e^{n\mu_0 T}$ for integer n . The origin of the higher harmonics is more complex. Our spike pattern formula works very well for other values of g^2/λ , with the requisite $\mu_0(g^2/\lambda)$.

Let us denote ζ_{pr} by $F_{NL}(\chi_i(\mathbf{x}))$. These are added to the conventional inflaton curvature fluctuations ζ_ϕ : $\zeta_{tot}(\mathbf{x}) \approx \zeta_\phi(\mathbf{x}) + F_{NL}(\chi(\mathbf{x})) - \langle F_{NL} \rangle$. (The ensemble average $\langle F_{NL} \rangle$ over all values of χ , is subtracted so ζ_{tot} fluctuates about zero.) Structure in χ_i and hence in F_{NL} , exists on a vast range of resolution scales, from k_{min} through k_h to k_e . Observed large scale structure (LSS), as probed by the CMB, redshift surveys, weak lensing, and rare event abundances such as of clusters probe ~ 10 e-folds in $\ln k$ below k_h^{-1} , and about the same number of e-folds just below this can be probed with the more uncertain astrophysical observables involving earlier stages in the nonlinear hierarchy, galaxies, dwarves, and the “first stars” within them. The superhorizon scales beyond k_h^{-1} have no impact on ζ_ϕ -structure, but do have a large impact on F_{NL} through the specific value $\chi_{>h}$ built from waves $k_{min} < k < k_h$. To explore the astrophysical consequences of F_{NL} , we marginalize over high frequency components χ_{HF} of $\chi \equiv \chi_{HF} + \chi_{LF}$ to form the conditional non-Gaussian “effective field”, $\langle F_{NL} | \chi_{LF} \rangle$, with ~ 40 -50 e-folds of “short distance” substructure in F_{NL} filtered out. The mean-field, $\langle F_{NL} | \chi_{LF} \rangle = \int F_{NL}(\chi) P(\chi | \chi_{LF}) d\chi$, is a Gaussian-smoothing of F_{NL} in field-space, via $P(\chi | \chi_{LF}) = \frac{\exp[-(\chi - \chi_{LF})^2 / (2\sigma_{HF}^2)]}{\sqrt{2\pi\sigma_{HF}^2}}$, with variance $\sigma_{HF}^2 = \langle \chi_{HF}^2 \rangle$. Using it will give reliable LSS inferences if the Fourier transform of the deviation $\Delta F_{NL} \equiv F_{NL} - \langle F_{NL} | \chi_{LF} \rangle$ is small for $k^{-1} \gg k_{LF}^{-1}$, the χ_{LF} filter scale. Since $\chi_{LF} = \chi_b + \chi_{>h}$ contains a spatially varying part χ_b built from waves with $k_h < k < k_{LF}$ and a constant superhorizon part $\chi_{>h}$. Which aspects of the spiky patterns of Fig. 1 that would be realized in our Hubble patch is quite dependent on the luck of our $\chi_{>h}$ -draw from a Gaussian distribution with variance $\sigma_{>h}^2 = \langle \chi_{>h}^2 \rangle$, in particular whether $\chi_{>h}$ is near a smoothed-peak, or small $\lesssim \sigma_{HF}$.

The analytic model, $F_{NL} = \sum_p F_p \exp[-(\chi - \chi_p)^2 / (2\gamma_p^2)]$, approximates each spike of Fig. 1 with

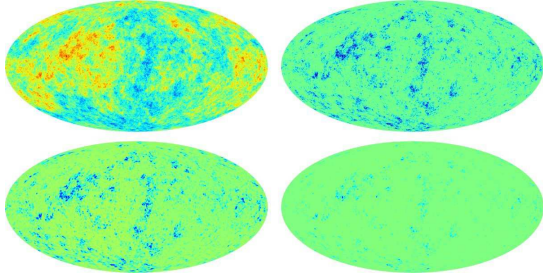


FIG. 3: Realizations of the nG map $\langle F_{\text{NL}}|\chi_b \rangle$ on the CMB sky. Top left shows a scale-invariant Gaussian random field realization $\chi_b(d_{\gamma\text{dec}}\hat{q})$ in direction \hat{q} on a sphere at the comoving distance to photon decoupling, $d_{\gamma\text{dec}}$. Top right shows the action of $\langle F_{\text{NL}}|\chi_b \rangle$ on it, using our Gaussian-line-profile approximation with 2 peaks at $\chi_p = \pm\nu_p\sigma_b$, for $\nu_p = 3.5$. Middle left shows the map convolved with a CMB transfer function, and smoothed on a 1° scale, right with $\nu_p = 4.5$; both show “cold spot” intermittency.

a Gaussian “line profile” of width γ_p centered on χ_p , with peak amplitude F_p and integrated line strength $u_p = F_p\sqrt{2\pi}\gamma_p$. The $\chi \rightarrow -\chi$ symmetry means that for each peak at χ_p there is a mirror peak at $-\chi_p$ of the same strength. The conditional n -point moments of F_{NL} , $\langle \prod_{i=1}^n F_{\text{NL}}(\mathbf{x}_i) | \chi_{\text{LF}} \rangle$ are then easily computable Gaussians, with quadratic terms in $\chi_i - \chi_p$ linked through the HF 2-point function of χ_{HF} . The mean field has $n = 1$:

$$\langle F_{\text{NL}} | \chi_{\text{LF}} \rangle = \sum_p U_p e^{-\frac{\chi_b^2(\mathbf{x})}{2\sigma_{p\text{HF}}^2}} \cosh\left\{ \frac{\chi_p > h}{\sigma_{p\text{HF}}^2} \chi_b(\mathbf{x}) \right\}. \quad (1)$$

Here $\sigma_{p\text{HF}}^2 = \gamma_p^2 + \sigma_{\text{HF}}^2$ is $\approx \sigma_{\text{HF}}^2$ for the typical γ_p we find and $U_p = \frac{2u_p\gamma_p}{\sigma_{p\text{HF}}} \exp\left\{-\frac{\chi_p > h}{2\sigma_{p\text{HF}}^2}\right\}$, with $\chi_p > h = \chi_p - \chi > h$. The χ_{HF} correlation function dependence of the fluctuation variance $\langle \Delta F_{\text{NL}}(\mathbf{x}_1) \Delta F_{\text{NL}}(\mathbf{x}_2) | \chi_{\text{LF}} \rangle$ precludes an analytic harmonic analysis, but we have investigated this numerically: *e.g.*, for a 1-spike version, this F_{NL} variance is 1% of $\langle F_{\text{NL}} | \chi_{\text{LF}} \rangle^2$ if it is smoothed on $\sim k_{\text{LF}}^{-1}$, and $\sim 0.1\%$ with $\sim 10k_{\text{LF}}^{-1}$ smoothing. (We have checked the effective field works even better for F_{NL} quadratic and exponential in χ .) The HF structure is very relevant to first-object formation, but what actually happens will be model-dependent. However, HF will not impinge upon LSS observables, since they are convolved with experimentally-determined or theoretically-imposed windows $\gg k_e^{-1}$ in scale.

A fundamental character of the resonant mechanism is the delay of in-arm preheating completion, translating into positive large excursions in $\delta \ln a|_H$. The associated perturbed Newtonian gravitational potential Φ_{N} is negative. The CMB sky temperature $T(\hat{q})$, an angular function of the CMB photon direction \hat{q} towards us, is a projected image of various sources whose 3D Fourier transforms involve various form factors $\mathcal{F}(|\mathbf{k}|)$ times $\Phi_{\text{N}}(\mathbf{k}, t_0)/3$. The dominant \mathcal{F} terms are from two CMB decoupling effects, and one late-time effect: the combined “naive Sachs-Wolfe (NSW) effect plus photon

compression-rarefaction”; the Doppler effect from flowing electrons; and the integrated Sachs-Wolfe (ISW) effect with \mathcal{F} a k -dependent time-integral of $6\dot{\Phi}_{\text{N}}/\Phi_{\text{N}}$ [1]. The upper panels in Fig. 3 correspond to $\mathcal{F} = 1$ and the lower panels are convolved with a CMB transfer function and smoothing on 1° , appropriate if the CMB sky is a direct map of the photon decoupling surface, ignoring its fuzziness (valid for the 1° smoothing) and a correct implementation of the ISW effect, which will affect the largest scales. However, the essential intermittent cold spot nature following from negative Φ_{N} will persist. Such cold spots will be polarized just as those deriving from ζ_ϕ are, and have a CMB spectrum, a prediction for the $\sim 6^\circ$ COBE/WMAP cold spot [7] if it is a smoothed remnant of resonant preheating.

Another non-intermittent nG regime is that of extreme “line blending”: Fig. 1 shows $f_\chi \chi_{\text{LF}}^2 / M_P^2$ with $f_\chi = 2 \times 10^6$ is a good fit to $\langle F_{\text{NL}} | \chi_{\text{LF}} \rangle$ below $\sim \sigma_{\text{HF}}$. (Such a quadratic form also follows from Eq. (1).) For $\chi > h \lesssim \sigma_{\text{HF}}$, we will get a power law in χ_b , $\beta_\chi \chi_b / M_P + f_\chi \chi_b^2 / M_P^2$, with $\beta_\chi = 2f_\chi \chi > h / M_P$. The conventional WMAP $-9 < f_{\text{NL}} < 111$ constraints [7] use $\sim \zeta_\phi + f_{\text{NL}} \zeta_\phi^2$. In our case, $f_\chi \chi^2$ is uncorrelated with ζ_ϕ^2 so the constraint on f_χ will be considerably relaxed, as long as the linear $\beta_\chi \chi_b$ term is subdominant to ζ_ϕ , as is expected.

Further exploration is needed of how spiked F_{NL} from resonant preheating may arise in more general inflation models and on the rich nG impact and observable constraints of such F_{NL} on short and long cosmic scales. For now, we note SUSY models provide light non-inflaton fields of the sort we need, and future CMB experiments could test whether nG cold spots are polarized. We thank A. Chambers, G. Felder, E. Komatsu, A. Linde and A. Rajantie for discussions.

-
- [1] J.R. Bond, *Theory and Observations of the Cosmic Background Radiation*, in Les Houches Session LX, ed. R. Schaeffer, Elsevier Science Press (1996); V. F. Mukhanov, *Physical Foundations of Cosmology*, Cambridge Univ. Press (2005); S. Weinberg, *Cosmology*, Cambridge University Press, (2008).
- [2] A. Linde and V. Mukhanov, Phys. Rev. **D56**, 535 (1997); D. Lyth and D. Wands, Phys. Lett. **B524**, 5 (2002).
- [3] G. Dvali, A. Gruzinov and M. Zaldarriaga, Phys. Rev. D **69**, 023505 (2004); L. Kofman, arXiv:astro-ph/0303614.
- [4] A. Chambers and Rajantie, Phys. Rev. Lett. **100**, 041302 (2008), arXiv:0710.4133.
- [5] P. Greene, L. Kofman, A. Linde and A. Starobinsky, Phys. Rev. **D56**, 6175 (1997).
- [6] A.A. Starobinsky, Phys. Lett. (1982); D. Salopek and J.R. Bond, Phys. Rev. **D42**, 3936 (1990); M. Sasaki and E.D. Stewart, Prog. Theor. Phys. **95**, 71 (1996).
- [7] E. Komatsu, et al., ApJS, **180**, 330 (2009); M. Cruz, E. Martinez-Gonzalez, P. Vielva, arXiv:astro-ph/0901.1986.
- [8] G. Felder and I. Tkachev, Comp. Phys. Comm. **178** 929 (2008).
- [9] A.V. Frolov, JCAP **0811**, 009 (2008).